sciendo

Polish Journal of Chemical Technology, 24, 4, 7—22, 10.2478/pjct-2022-0024

Investigation and Prediction of ECMM characteristics of Hardened Die Steel with Nanoparticle Added Electrolytes Using Hybrid Deep Neural Network

Vijayakumar Kanniyappan[1*], Sekar Tamilperuvalathan[2]

[1]*Department of Mechanical Engineering, TPEVR Government Polytechnic College, Vellore-632002, India*
[2]*Department of Mechanical Engineering, Government College of Technology, Coimbatore, 641013, India*
[*]*Corresponding author: e-mail: kvtpevr@gmail.com*

In our work, the process efficiency of the ECMM should be improved by using different combinations of nanoparticles and added electrolytes. The superior aim of this work is to improve and predict the ECMM machining characteristics of die hardened steel, namely material removal rate (MRR), Tool wear rate (TWR) and Surface Roughness (Ra). The machining conditions are optimized using Response Surface Methodology (RSM) based on Box Behnken Design. The better Nano electrolyte is optimized using Deer Hunting Optimization (DHO) based on the machined outcomes, and the performances are predicted using a hybrid Deep Neural Network (DNN) based DHO. The hybrid DNN-DHO based predicted outcome of MRR is 0.361 mg/min, TWR is 0.272 mg/min and Ra is 2.511 μm. The validation results show that our proposed DNN-DHO model performed well and obtained above 0.99 regression for both training and validation of DNN-DHO, where the root mean square error ranges between 0.018 and 0.024.

Keywords: ECMM, Die hardened steel, machining parameters, RSM, hybrid, neural network, prediction.

INTRODUCTION

Nowadays, the machining of hardened steel is mostly adapted by many nontraditional methods such as Laser beam machining, Electric discharge machining (EDM), etc.[1]. When using nontraditional methods, certain debris attained in the machining gap cannot be removed quickly and may provide a minimal material removal rate (MRR). Electrochemical machining (ECM) is a process in which anodic dissolution based chemical activity is mainly responsible for material removal irrespective of material hardness[2]. When using the ECM process for machining the structure in the ranges of 1 to 999 μm is known as electrochemical micromachining (ECMM). ECMM offers several beneficial activities such as tool wear reduction, the ability to machine hardened and high strength materials, and promoting smooth surfaces[3, 4]. Besides, greater material removal rate, quicker machining period, environmentally friendly behavior, and allowing the machining of chemically resistant materials such as super alloys, stainless steel, copper alloys, etc. Normally, steel and its alloy are generally considered weak materials due to their greater chemically reactive behavior. Thus, it leads to premature failure of the tool during the machining operation[5].

Electrochemical micromachining (ECMM) is considered a non-conventional approach, and the machining process is completely performed by the anodic dissolution behavior of the workpiece. In ECMM, the workpiece and tool electrode get entirely submerged in an electrically conductive electrolyte such as water, sodium hydroxide, Sodium nitrite, etc.[6]. Here, the workpiece is specified as a positive electrode (anode), and the constant potential is given to the two electrodes. Such given potentials make the DC flow between the electrodes and dissolve the anode material. At the cathode, the reaction happened due to hydrogen gas generation[7, 8]. The electrolysis is the movement of the current through an electrically conductive medium between two electrodes which ends the circuit connection. The water-dependent solution is usually often used as an operating electrolyte. Anasane and Bhattacharyya[9] investigated EMM machining on titanium by varying the electrolytes to determine its suitability. Seven different electrolytes (2 non-aqueous and 7 aqueous) are used to select the better-operating electrolytes based on the EMM machining performances. The author concluded that the titanium micromachining characteristics were outperformed for the non-aqueous based electrolyte combination, namely sodium bromide and ethylene glycol. Thanigaivelan et al.[10] have investigated the influences of various $NaNO_3$ electrolytic concentrations. By keeping constant electrolyte temperature at 37±0.5 °C and 1A current throughout the experiment. The author found that 35 gm/l of electrolytic concentration produced better ECMM machinability of copper with a good surface finish.

At the time of ECMM machining on steel alloy, a Passive oxide film, which develops during the anodizing phase when using water as an electrolyte, quickly avoids uniform dissolution and creates a rugged surface layer. Such a drawback gets minimized by using an acid electrolyte, this helps to prevent the formation of the precipitate by solving the insoluble waste agents[11]. Geethapriyan, T. et al.[12] used NaCl as an electrolyte during ECMM operation of stainless steel-316 material and obtained a maximum of 1.345 mg/min of MRR with 346.912 μm overcut at 0.5 g/l electrolyte concentration and 20 V voltage supply. Bhuyan, B.K. and Yadava, V.[13], studied the electrochemical spark machining of borosilicate glass material using NaOH electrolyte and brass cutting wire and achieved significant performance. Moreover, Sethi, A. et al.[14] proposed a new eco-friendly electrolyte combining citric acid and $NaNO_3$. The author attained better surface quality with effective microwire-ECMM operation on an alloy of tungsten carbide and cobalt material. Although acidic electrolytes help with precipitate reduction, they may affect the efficiency of the machining operation. To minimize all these issues,

nanoparticles were added to the electrolytes such as NaOH, NaCl, $NaNO_3$, etc.[15].

Once the nanoparticles are immersed in the electrolyte, the experiment's total electrical conductivity enhances, and the material removal activity becomes more effective. Because the high conductivity of the nanoparticle enhances the processing parameters and the machining accuracy[16, 17], another justification for increased material removal efficiency is the nanoparticle metal ions. In comparison, the usage of nanoparticles tended to reduce the overcut as compared to the electrolytes with an absence of nanoparticles. So, it allows us to increase the precision of machining parameters[18]. Sekar et al.[19] utilized the copper particles suspended NaCl electrolyte to analyze die-hardened steel's ECM machining analysis. The improved performances of MRR and surface roughness rates were achieved because of the contribution of nanoparticles since the nanoparticles help to break the gas layer attained in the inter-electrode gap. Jiang et al.[20] performed vibration-assisted wire electrochemical micromachining (WECCM) for machining microgrooves using sodium nitride electrolyte with B_4C particles. The experimental findings indicate that the introduction of B_4C particles not only decreased the accumulated electrolytic products on the cathode wire surface. But also avoided the formation of bubbles in the machining gap zone and increased the surface strength of the microgrooves. Another author Geethapriyan T et al.[21], used copper nanoparticles and added $NaNO_3$ electrolyte solution in the ECMM process. The experiment was conducted to machine 430 grade stainless steel material with copper cutting wire. The author reported that the copper nanoparticle added $NaNO_3$ electrolyte enhanced the localization region and surface quality with less stray current effect. The higher thermal conductivity of nanoparticle suspended $NaNO_3$ produced better MRR and overcut than neat $NaNO_3$ electrolyte. Moreover, Vinod Kumaar, J.R. et al.[22] found better ECMM output performances while producing micro holes in 316 L grade stainless steel using copper nanopowder suspended citric acid electrolyte.

Even though machining output has been improved by choosing optimum process circumstances, the precision of machining, particularly the quality of the surface, always requires more enhancement for engineering applications[23]. Hence, some authors did several optimization methods such as Taguchi, Deep neural network model, hybrid optimization algorithms etc., to prefer the better target based on the performances. This multi-objective method helps to promote a more efficient selective parameter from the outcomes[24, 25]. Pradeep et al.[26] experimented on ECMM using the electrode made of polymer Graphite to produce the greater aspect ratio based micro holes. ASTM A240 type stainless steel machining is comparatively studied based on cryogenically untreated and treated polymer graphite electrodes. The author used a multi-objective cuckoo search algorithm (MOCS) optimization method to finalize cryogenically treated electrodes' superior performance. Krishnan, N. et al.[27] proposed the L16 orthogonal array Taguchi method for multi-response optimization of ECMM. The author obtained optimal results at 80% duty cycle, 600 rpm rotational speed, 21V of the voltage supply, 0.2M electrolyte concentration and 0.8 μm/s feed rate during the experimentation. After analyzing the confirmatory test, the model attained a 0.245 performance grade improvement action. Another multi-response optimization of the ECMM process was done by Panigrahi D. et al.[28] using the Particle Swarm Optimization algorithm (PSO). The author utilized response surface methodology (RSM) to design the experiment model. After investigation, the author noticed that the optimized values were closer to the experimental outcomes. Moreover, Prakash, J. and Gopalakannan, S.,[29], Ranganayakulu, J., et al.[30] and Gautam, N., et al.[31] have studied different optimization methods like Teaching-Learning-Based Optimization (TLBO) algorithm, Graph theory algorithm (GTA), Taguchi, RSM, PSO and Genetic algorithms etc., and found better accuracy with less root mean square error values.

Based on the literature, many authors did experimentation on ECMM of ceramics like titanium, glass, different grades of stainless steel, etc. But the ECMM investigation with hardened die steel material was very rate. Due to the large applications of these hardened die steel materials in surgical instruments, nozzles, etc., the finishing of such products should be neat and precise. But, the precise micromachining of hardened die steel with the conventional machining method was impossible. Hence, this study mainly focused on determining the ECMM performances of hardened die steel because hardened die steels are very hard and brittle materials. However, the efficiency of the ECMM process was improvised by some authors by utilizing different electrolyte solutions individually. In our work, two different electrolytes of $NaNO_3$ and NaCl were combined to produce a more effective electrolysis process. However, in previous studies, the authors suspended different nanoparticles, such as copper nanopowder, B_4C nanoparticles, etc., in the electrolyte to enhance the thermal conductivity of the electrolyte. The influence of hybrid nanoparticle suspended electrolytes was not yet investigated. In this study, combining two different nanoparticles was added to our proposed electrolyte solutions to enhance our novelty. Moreover, recently, researchers have analyzed the optimization performance of different machine learning algorithms. The ECMM parameter optimization and prediction behavior of our own hybrid Deep Neural Network based Deer Hunting Optimization algorithm was also comparatively studied.

The supreme contributions of this research work are listed below,

– To study the influence of different ZnO and SnO_2 nanoparticles, added NaCl and $NaNO_3$ electrolytes during ECMM of hardened die steel.

– To obtain the optimal nanoparticle added electrolyte from 6 electrolytes by ECMM process.

– To study the influence of input process parameters such as electrolytic concentration, supply voltage and duty cycle in ECMM performance.

To optimize the ECMM process parameters by using RSM-BBD and hybrid DNN-DHO algorithm.

– To evaluate the prediction performance of the proposed hybrid DNN-DHO algorithm in the ECMM process.

In this work, MATERIALS AND METHODOLOGY explains the proposed methodology, materials used during experimentation, and nanoparticle added electrolyte

preparation process. OPTIMIZATION AND PREDICTION METHODS provides detailed information about response surface methodology and hybrid deep neural network based DHO design. The major result obtained from the DNN-DHO, RSM prediction and experimentation are given in RESULT AND DISCUSSION section and concluded at CONCLUSION as well.

MATERIALS AND METHODOLOGY

Materials used

In our work, the Tungsten carbide tool with a diameter of 150 microns is used to drill the hardened die steel by electrochemical micromachining technique. Here, the electrolyte without nanoparticles and nanoparticles are used comparatively. The nanoparticles such as zinc oxide (ZnO) and stannic oxide (oxides of tin or SnO_2) are introduced with the electrolyte to improve the machining characteristics. Also, two different electrolytes, namely NaCl and $NaNO_3$, were investigated.

Experiment planning

The step-by-step procedure of the proposed work is given in Figure 1. In this work, the electrochemical micromachining operation is initially held on the hardened die steel by making the micro holes. This process is achieved in two stages:

(i) The absence of nanoparticles in electrolyte

(ii) Nanoparticles added electrolytes.

The experiment design is planned by using the box Behnken approach from RSM. By using the obtained experimental results, the RSM and neural network models were trained. Finally, the hybrid deep neural network-based DHO prediction method is performed to forecast the optimized performances.

Experiment setup and procedure

In this proposed work, the electrochemical micromachining of die hardened steel occurs by handling the drilling operation. The experiment is conducted by varying the voltage, duty cycle, and electrolytic concentration, and the machining outputs such as MRR (mg/min), TWR (mg/min), and surface roughness (μm) are analyzed. The ECMM machining process is demonstrated in Figures 2 and 3. The nanoparticles added to electrolytic combinations are stored in the electrolytic tank, providing efficient flushing activity during machining through the pump. In this, the workpiece made of hardened die steel act as an anode and the tungsten carbide tool electrode act as a cathode. In the workpiece, manual movement is achieved by moving it in an x-y direction, and a fixture holds the workpiece. The tool movement as z-direction is achieved with a stepper motor, and the cathode tool is fixed with this stepper motor. The amount of DC supply is provided between the tool and the workpiece. Figure

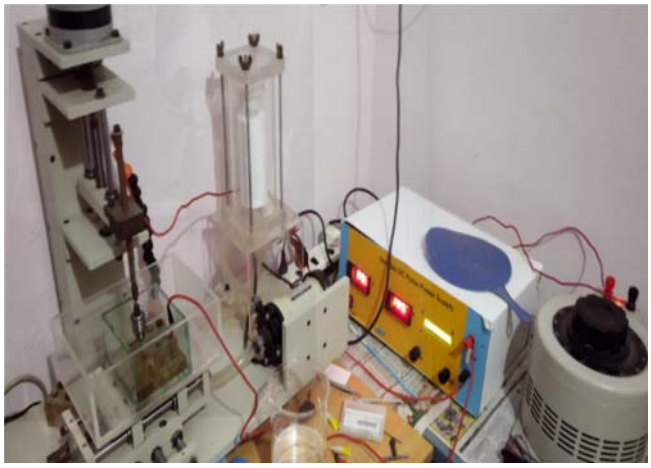

Figure 2. ECMM Experimental Setup

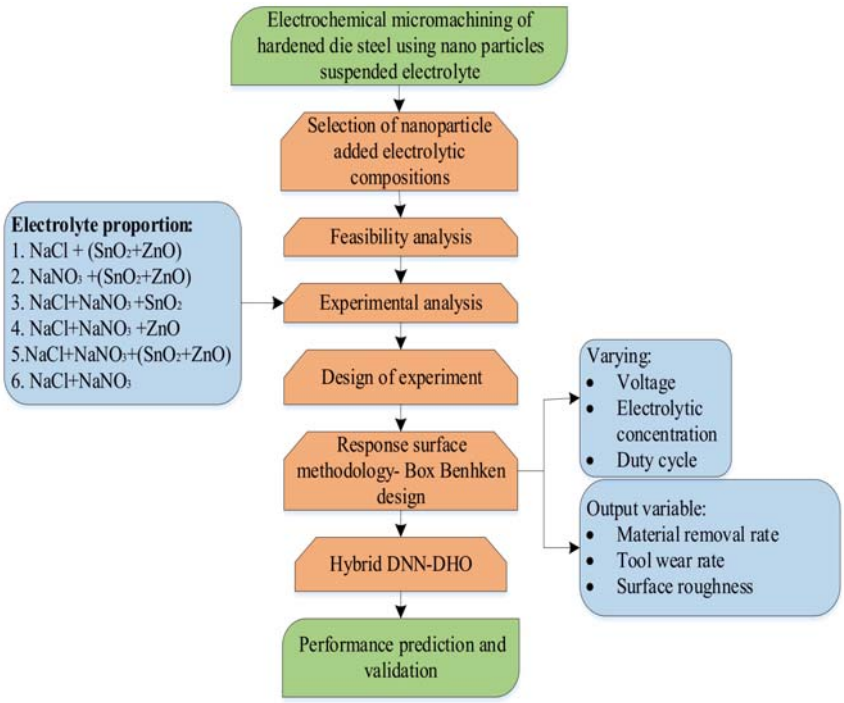

Figure 1. Proposed scheme of Research Work

(a) ECMM Machining (b) Machined work piece

Figure 3. ECMM machining of Die Hardened Steel

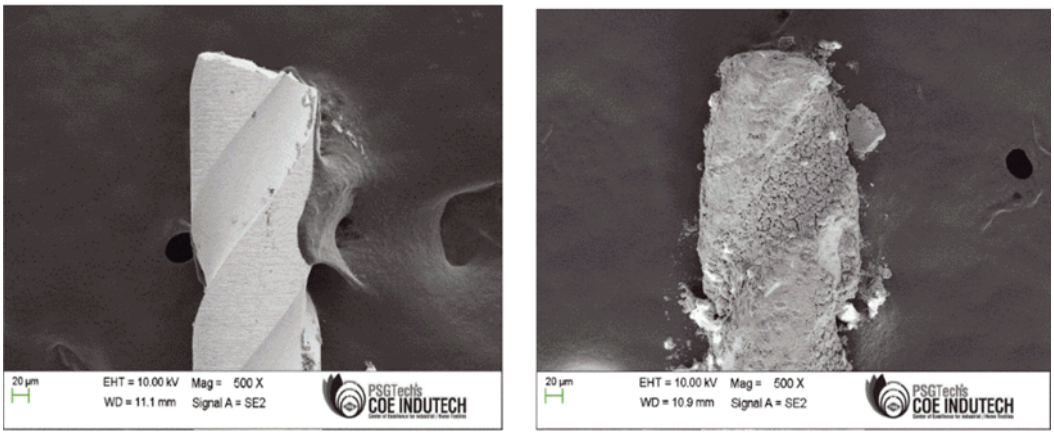

(a) Before machining (b) After Machining

Figure 4. SEM Analysis of tool

(a) Before machining (b) After machining

Figure 5. SEM Analysis of before and after the machined workpiece

4 and 5 represents the SEM analysis of before and after machining of the tool and workpiece. The SEM analysis reveals that the wear rates have participated in the tool during machining.

Nano fluid preparation

The properties of ECMM electrolytes get because of the contribution of nanoparticles. The machining characteristics, namely MRR, and surface roughness, depend mainly on the thermal conductivity behavior. The contribution of nanoparticles helps to enhance thermal conductivity, and it tends to improve machining properties. In other words, it helps to enhance the electron availability on the tool surface and the electrolyte. Normally, the nanoparticles, such as the oxides of aluminium, copper, silver, etc., are attained in the nanofluids at less than 100 nm. The increased size of suspended particles may tend to clog the flow channel of electrolytes. However, some investigations were done on the separate inclusion of different nanoparticles in various electrolytes. Based on the literature, the investigation of ECMM with ZnO and SnO_2 nanoparticle suspended electrolyte was not yet done. This investigation uses six combinations of ZnO and SnO_2 nano electrolytic blends to identify the optimal electrolyte blend. Because the selected ZnO and SnO_2 nanoparticles have high thermal and electrical conductivity, which may improve the efficiency of ECMM of hardened die steel by using NaCl and $NaNO_3$. For the entire combinations, 20, 25 and 30 g/l of electrolytic concentrations are utilized, in which 5 grams of nano-

particles are added for the entire mix proportions. The nanoparticles in the electrolytes are continuously stirred

Table 1. Electrolytic combinations

Electrolyte	Nanoparticles
$NaCl+NaNO_3$	–
$NaCl+NaNO_3$	Stannic oxide+zinc oxide
NaCl	Stannic oxide+zincoxide
$NaNO_3$	Stannic oxide+ zincoxide
$NaCl+NaNO_3$	Stannic oxide
$NaCl+NaNO_3$	Zinc oxide

Table 2. Properties of Electrolytes

Electrolytic properties	Nanoparticles added electrolyte	Neat Electrolyte
Solidity	31	44
Turbidity (NTU)	nil	nil
pH value	8.5	8
Electrical conductivity	17	14.4

to avoid the action of sedimentation. The electrolytic combinations used in this research work are given in Table 1. The properties of nano electrolytic fluid are given in Table 2.

OPTIMIZATION AND PREDICTION METHODS

Response surface methodology

The formulation of mathematical correlations to optimize, forecast, simulate and model the statistical design of the experiment using independent and dependent variables of MRR, TWR, Ra and electrolyte concentration voltage and duty cycle in the tool of RSM[32, 33]. It defines the optimum solution in the corresponding region, which includes the range of input factors and responses from the machining system. This method uses a polynomial equation for mathematical interactions between factors and responses. The machining result from the system is highly influenced by these factors, which are hard to define in the linear method. Hence the quadratic correlation is used to reveal the response function.

$$Z = \beta_0 + \sum_{i=1}^{k} \beta_i y_i + \sum_{i=1}^{k} \beta_{ii} y_i^2 + \sum_{i=1}^{k} \sum_{j=i+1}^{k} \beta_{ij} y_{ij} \quad (1)$$

In the equation, the response is represented as Z; the intercepts, first order, linear, and quadratic coefficient are $\beta_0, \beta_i, \beta_{ii}, \beta_{ij}$ respectively. The ANOVA is used to evaluate the responses, giving the statistical design significance. This work considered the experiment at seventeen runs of experiment progressed in design expert software. The three factors and level of the experiment are designed in

Table 3. Factors and ranges of parameters

Code	Variables	Unit	Range	
			Low	High
A	Electrolytic Concentration	(g/l)	20	30
B	Voltage	(V)	17	19
C	Duty Cycle	(%)	30	50

Box Behnken design. The design evaluates the probability value (p-value) and determination/regression coefficient (R^2) to determine the significance. The independent variable and its level range are given in Table 3.

Hybrid DNN-DHO

The artificial neural network-based network, which consists of multiple hidden and visible layers, is called a deep neural network. This network consists of functions, biases, neurons, and weights. The new state of the art in the prediction and classification of a large number of data with high accuracy is possible using deep neural networks[34]. This work uses DNN to predict the machining performance of the ECMM hardened die steel. This network's testing, training and validation predict performances from the machining parameters. Process parameters of electrolytic concentration, voltage, and duty cycle are given in the input layer, which is moved to the hidden layer then the predicted outputs are obtained from the output layer, respectively. The layout of DNN is given in Figure 6.

In this network, the signal generation between inputs to the output layer is done by some neurons. They use the activation function to transform these signals. The size of the input vector is given as

$$x = [x(k), x(k-1), \ldots x(k-m)] \quad (2)$$

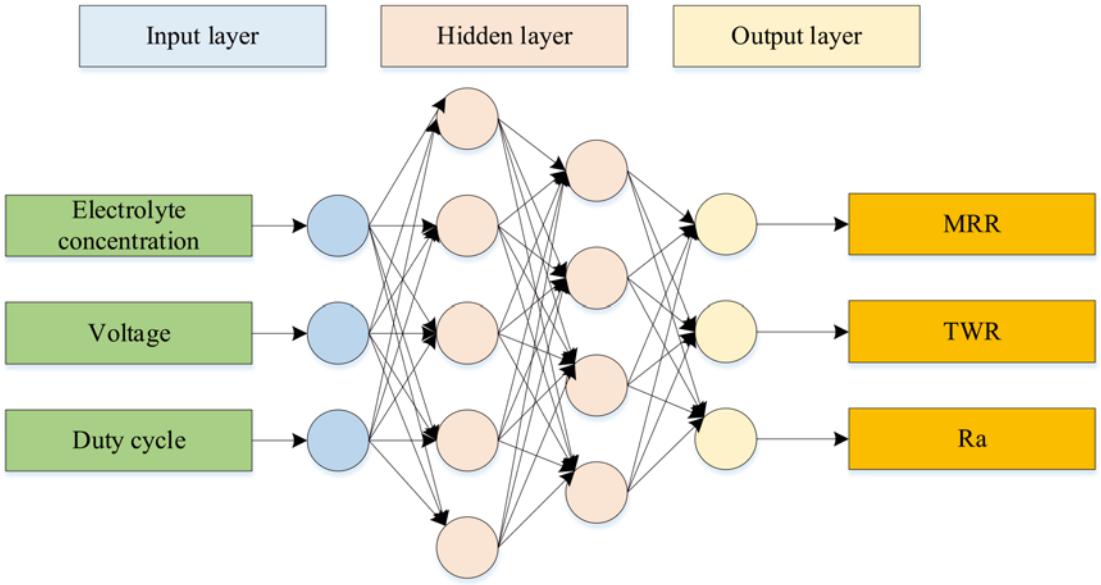

Figure 6. Layout of neural network

$x(k+1)$ is used to predict the input values. In the hidden layer, the weights are calculated by using the equation

$$x_j = \sum_i^m x_i * w_{ij} + \theta_j \quad (3)$$

Where w_{ij} the weight obtained from the nodes, θ is biased and x_i denotes inputs. Then the activation function is

$$\sigma_j(X) = \exp\left[-\left(x-\mu_j\right)\right]/\gamma_j^2 \quad (4)$$

Where X is an input vector, $\mu_j - \gamma_j$ is the network width and centre, and the $\sigma_j(x)$ represented activation function of j^{th} neuron. The output variables are predicted during the training stage of DNN. The normalization of error values also is performed in this stage, and it is continued till the minimum error value is achieved. And the weight of the nodes is updated based on the error values. The weight is updated randomly using

$$\Delta w_{ij} = -n\frac{\theta_E}{\partial w_{ij}} \quad (5)$$

In the equation, the learning rate is denoted as n, and error values are E. During this updation, the random values are selected, so the efficiency of the network will be affected, and the prediction output becomes an error. And hence these values are getting optimized by using a deer hunting optimization algorithm, and the method of weight updation is explained. The main importance of this algorithm is improving efficiency by reducing error using the weight optimization technique.

Deer hunting optimization

The deer hunting action performed by humans is the major role of DHO, based on the desired optimal position. In our work, the weight values formed from the DNN are considered humans, and the small error values are considered Deer[35]. In other words, the weight values are selected based on the minimized error.

Initialization of population:

The initialization behavior of weight value is achieved based on the following expressions,

$$X = \{X_1, X_2, ...X_3\} \quad 1 < j \le n \quad (6)$$

Where, the total weights are denoted as n, which acts as a solution in population X.

Exploration stage:

In this exploration stage, the minimal error values are determined based on position updating for the weight values. Two characters, such as leaders and successors, are attained in the entire weight values. Here, the successor mainly contributes to selecting the best minimal error values. The position of the succeeding and the first best weight values are represented as $X^{succesor}$ and X^{lead}.

(i) Leaders position,

Each weight tries to achieve the best position during the position updating procedure.

$$X_{i+1} = X^{lead} - Y.k.\left|L \times X^{lead} - X_i\right| \quad (7)$$

Where X_i and X_{i+1} represents the position of the current and the next iterations.

The vector coefficients are denoted as L and Y, and the random number k is generated in the ranges of 0 and 2.

The coefficient vectors, $Y = \frac{1}{4}\log\left(i + \frac{1}{i_{max}}\right)b \quad (8)$

$$L = 2.c \quad (9)$$

Here, the random number c is in the intervals of 0 and 1, and the parameter b ranges between –1 and 1. The maximum iteration is denoted as i_{max}.

The position of the error values varies based on the weight values position. In other words, the position of weight values varies until it reaches the best position to reach the minimal error values. This behavior is achieved by adjusting the parameter of Y and L.

(ii) Position of successor

This is an active exploration stage; in this stage, the weight values are more effectively attained for determining the minimal error values. The adjusting of the L vector (vector $L<1$) mainly contributed to achieving the optimal position. So, the updating of the successor position is superior to updating the position of the first best position. Therefore, the global searching equation is expressed as,

$$X_{i+1} = X^{successor} - Y.k.\left|L \times X^{successor} - X_i\right| \quad (10)$$

For the weight values, the successor position is represented as $X^{succesor}$.

Here, optimal minimized error values are determined mainly by adjusting L. The random and the best-minimized error values are selected using $L<1$and when $L>1$. The optimized machining performances were re-obtained from the algorithm with minimal error.

RESULT AND DISCUSSION

Effect of Nanofluid on machining performance

The electrochemical micromachining performance of the drilling operation is conducted on the hardened die steel. The experimentation is performed under the six different combinations of electrolytes with nanoparticles. The major influence of different electrolyte concentrations on the machining performance is analyzed. Figure 7 represents the experimented machining performances of various nanofluids in hardened steel. It depicts that the MRR increases with increasing the electrolytic concentration. Nanoparticle added fluid concerns the increase of MRR at a high electrolyte concentration at 25 g/l; beyond this amount, it tends to be reduced slightly. Figure 7(b) shows the tool wear rate decreases with the increase in electrolyte concentration. The proportion of nanoparticles in electrolyte gives the decreasing factor of tool wear at high concentrations and high voltages. Similar results were obtained by Elhami, S. and Razfar, M.R.[36], while adding Al_2O_3 and Cu nanoparticles to NaOH electrolyte solution. The high material removal rate affects the surface finish of the material, and also, high temperature has the possibility of increasing tool wear. The increase of surface roughness with the increase of electrolyte concentration is given in Figure 7(c). A good combination of electrolytes achieves a better reaction between the workpiece and tool. It also performs the removal of a chip on the workpiece surface.

The optimum performance condition is achieved by combining NaCl with stannic and zinc oxide. The Stannic

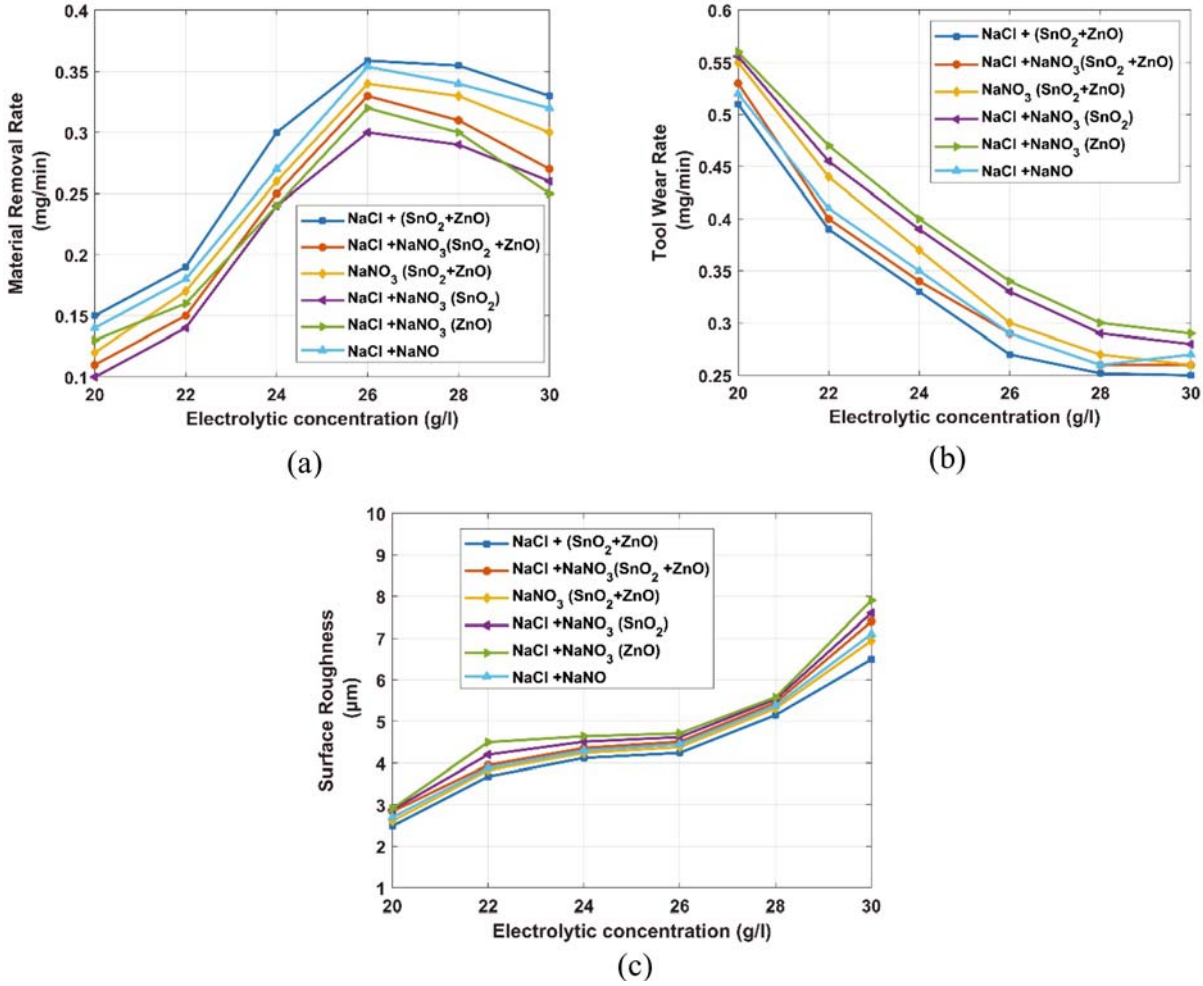

Figure 7. Experimented results for various electrolyte fluids a) MRR, b) TWR, c) Ra

oxide and zinc oxide added NaCl electrolytic solution outperforms the other electrolyte combinations. However, the wear rate is optimal for the NaCl and $NaNO_3$ solution. This is because, when adding nanoparticles to the electrolytes, thermal conductivity gets improved, so the attainable wear rate gets enhanced. The machining characteristics such as surface roughness and tool wear rate are optimal for the nanoparticles added NaCl. When using NaCl, the maximum mass transfer dissolution of die hardened steel happens. The increased mass dissolution of the workpiece increases the flow of voltage. At the same time, the contribution of $NaNO_3$ during the machining process promotes moderate behaviors compared to NaCl due to its minimal thermal conductivity. When using the NaCl and $NaNO_3$ combination, the outcoming performances are similar or quite varied to applying NaCl electrolyte.

Experimental results analysis

The experiment is designed on the response surface methodology of box Behnken design with 17 experimental runs. The optimum condition obtained from the electrolyte suspended with nanoparticle is given to the statistical analysis. Compared to the other electrolyte combination, the best performances are obtained from the Stannic oxide (SnO_2), and zinc oxide (ZnO) added to NaCl electrolytic solution. Besides the influence of Nanoparticles, smashing the insulation layer lies between the tool and workpiece and enhances the machining behaviors. Using this NaCl+SnO_2+ZnO electrolyte, the workpiece was machined in an ECMM machine at different input levels of voltage, electrolytic concentration and duty cycle. 17 input parameter combinations, including 5 repeated input combinations, were obtained from RSM-BBD. And their respective ECMM output (MRR, TWR and Ra) values were observed and tabulated. The influence of experimental parameters on the performance is given in Table 4.

The polynomial equation for the analysis of ECMM parameters is explained below. The MRR, TWR, and Ra model is developed based on this equation. The response factors are analyzed by using this equation.

$$MRR = -1143.68750 - 7.01250\,A + 132.15000\,B - 0.478750\,C + 0.015000\,AB + 0.070000\,AC - 0.117500\,BC + 0.096000\,A^2 - 3.32500\,B^2 + 0.006000\,C^2 \quad (11)$$

$$\mathbf{TWR} = -80.70000 - 9.78750\,A + 44.83750\,B - 4.08250\,C + 0.155000\,AB + 0.060000\,AC + 0.025000\,BC + 0.084500\,A^2 - 1.63750\,B^2 + 0.030875\,C^2 \quad (12)$$

$$\mathbf{Ra} = +50.24637 - 0.139750\,A - 4.67237\,B - 0.218237\,C - 0.006500\,AB - 0.000150\,AC + 0.007575\,BC + 0.000885\,A^2 + 0.135375\,B^2 + 0.002204\,C^2 \quad (13)$$

Where, *A* represents the concentration of electrolyte in g/l, *B* represents the amount of voltage supply in terms of *V*, and *C* denotes the percentage of duty cycle, respectively.

The above equations predict the response from the given input variables. The effectiveness of the lacked

Table 4. ECMM machining parameters when using NaCl + SnO_2 + ZnO electrolyte

Exp. No	A:Electrolytic Concentration (g/l)	B: Voltage (V)	C: Duty Cycle (%)	Material Removal Rate mg/min	Tool Wear Rate mg/min	Surface Roughness µm
1	20	19	40	0.281	0.300	5.760
2	20	17	40	0.132	0.501	5.051
3	30	19	40	0.353	0.284	3.684
4	25	18	40	0.251	0.383	4.242
5	20	18	30	0.300	0.440	4.831
6	25	17	30	0.162	0.461	3.323
7	30	18	50	0.332	0.483	4.125
8	25	17	50	0.113	0.510	5.153
9	30	17	40	0.201	0.452	3.133
10	30	18	30	0.334	0.341	2.492
11	25	18	40	0.248	0.383	4.241
12	25	18	40	0.252	0.372	4.242
13	25	18	40	0.249	0.383	4.240
14	25	19	30	0.359	0.270	3.890
15	20	18	50	0.162	0.462	6.493
16	25	18	40	0.251	0.382	4.244
17	25	19	50	0.264	0.334	6.023

fit values for the experimented values is validated by using the ANOVA. The ANOVA response for the MRR, TWR and SR are categorized in Tables 5 & 6. From the tables, it reveals that the obtained p = values are less than 0.0001, and it makes the system more significant. In this, voltage is majorly contributed to influencing the machining performances. The acceptability of the designed model is justified by performing the fisher test or *F* ratio. It is applied in the lack of fit of the model if the probability of *F* value is less than 0.05 gives the significant term. Otherwise, the model is insignificant.

The perturbation effect of MRR by considering the entire input conditions, namely voltage, electrolytic concentration and duty cycle, are given in Figure 8. The figure shows that the maximum material removal rate is obtained at the maximum voltage level. The increasing voltage level tends to maximize the melting behavior of the material and impetuous forces, so more material gets removed from the machined zone. During machining, the formation of disturbing gas layers is broken by the assistance of nanoparticles, so the smooth MRR machining behavior is maintained.

Table 5. ANOVA of response variables

Variables	MRR		TWR		Ra	
	f- value	p-value	f- value	p-value	f- value	p-value
Model	106.05	< 0.0001	173.56	< 0.0001	115.26	< 0.0001
A-Electrolytic concentration	155.21	< 0.0001	47.64	0.0002	569.61	< 0.0001
B-Voltage	557.39	< 0.0001	1171.93	< 0.0001	55.70	0.0001
C- Duty cycle	111.72	< 0.0001	156.44	< 0.0001	392.27	< 0.0001
AB	0.0237	0.8819	4.12	0.0818	0.2520	0.6310
AC	51.72	0.0002	61.80	0.0001	0.0134	0.9110
BC	5.83	0.0465	0.4292	0.5333	1.37	0.2802
A^2	25.60	0.0015	32.26	0.0008	0.1230	0.7362
B^2	49.13	0.0002	19.38	0.0031	4.60	0.0691
C^2	1.60	0.2464	68.91	< 0.0001	12.20	0.0101
Lack of fit	–	–	5.46	0.0673	–	–
P<0.05= significant, p> 0.05 insignificant						

Table 6. Statistical result

Response	SD	Mean	R^2	Adj R^2
MRR	0.0098	24.85	0.9927	0.9834
TWR	0.0076	39.48	0.9955	0.9898
Ra	0.1295	4.42	0.9933	0.9847

* R^2 – Regression coefficient; SD – Standard deviation; Adj R^2 – adjusted R^2

Parametric Effect of MRR

The ratio of the removed volume of material to the total machining time is called the material removal rate (MRR). Before starting the analysis of MRR, the non-machined workpieces are weighed and compared with the weight of the machined workpiece. The MRR rate is calculated from equation 14,

$$MRR = \frac{W_{bf} - W_{af}}{T} (mg/\min) \quad (14)$$

Where, before and after machining of workpiece weights are given as W_{bf} and W_{af}, the machining time is represented as *T*.

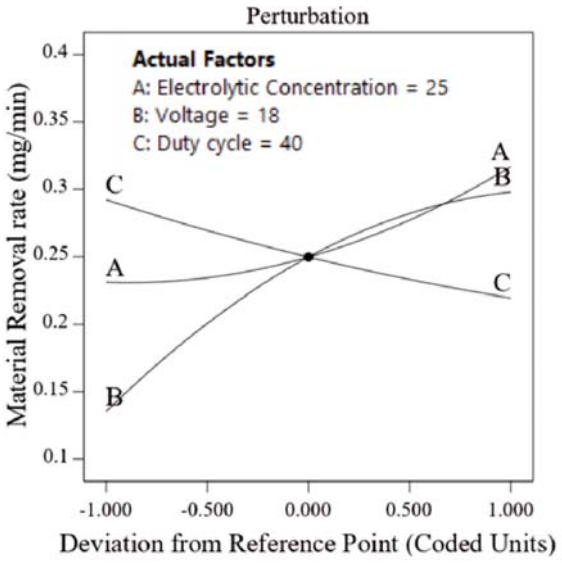

Figure 8. MRR perturbation

Figure 9 demonstrates the 3-D Plots for analyzing the interrelation between the input machining conditions with the MRR rate. The influence of voltage and electrolytic concentration on MRR rate is given in Figure 9(a). By comparing the electrolytic concentration, voltage efficiently enhances the material removal rate. The decreased MRR rate is achieved due to the enhanced chemical reaction of electrolytic concentration. Teimouri, R. and Sohrabpoor, H. also observed similar results by varying the voltage and electrolyte concentration[37]. At the maximum voltage level of 19 V and the maximum electrolyte concentration of 30 g/l, the highest MRR of 0.359 mg/min is achieved.

Figure 9 (b) represents the interaction of duty cycle electrolytic concentration over MRR. Compared to the duty cycle, quite greater performances are obtained due to the increase in Electrolytic concentration. By increasing the duty cycle, the MRR rate is increased because of the ability to increase the heat transfer rate. The maximum MRR of 0.332 mg/min is obtained at the increased electrolytic concentration of 30 g/l and duty cycle of 50%. The relationship between the voltage and the duty cycle for the MRR rate is given in Figure 9(c). At increased voltage conditions, the MRR rate is higher than the duty cycle. Improving the voltage levels increases the workpiece surface's temperature, which tends to enhance the MRR characteristics[27, 28, 22, and 40]. At the voltage of 19 V and the duty cycle of 30%, the maximum MRR obtained in the experimentation is 0.36 mg/min.

Tool Wear Rate

Tool wear rate is the measure of the difference between the weight of the before machined and after machined tool with respect to time. The rate of wear that occurs with the tool is comparatively less than the workpiece. The TWR rate is calculated by using equation 15,

$$TWR = \frac{E_{bf} - E_{af}}{T} \ (mg/\min) \tag{15}$$

Where, before and after machining of tool weights are given as E_{bf} and E_{af}, the machining time is represented as T.

By increasing the voltage, the tool wear rate gets reduced. At the same time, the duty cycle and electrolytic concentration are directly proportional to the tool wear rate. Charak, A. and Jawalkar, C.S.[38], have also found

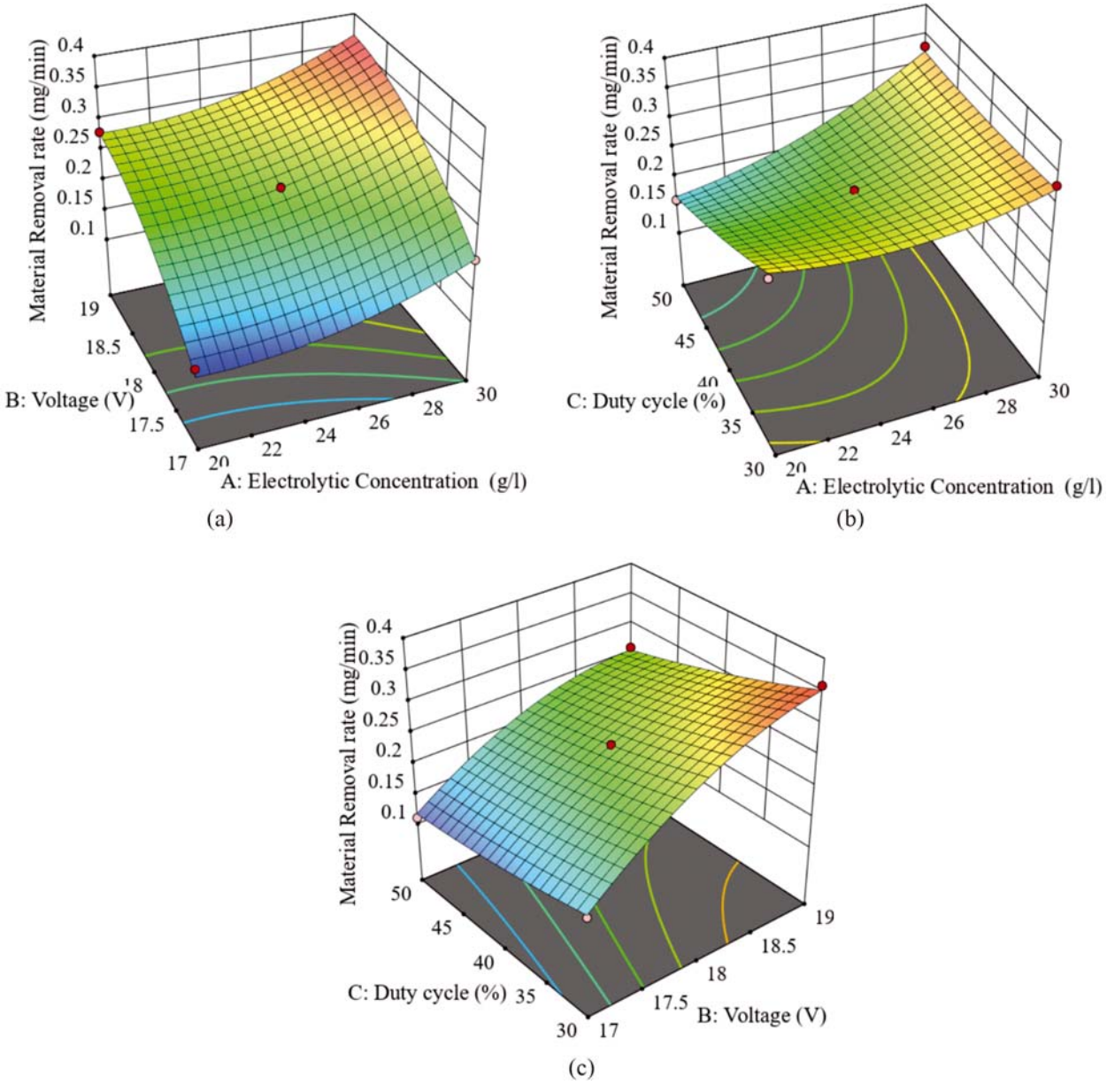

Figure 9. 3-D Surface plots for analyzing the effect of input parameters on MRR

a significant reduction in toot wear at lower electrolytic concentrations. The machining tool's high carbon content is one reason for wear reduction. This is due to a high temperature of machining. The heat generated during machining diffuses into the spaces and decomposes the dielectric fluid's carbon at a very high temperature. The part of decomposed carbon got deposited around the electrode, preventing it from wearing. The perturbation effect of tool wear rate with respect to its input machining parameters is given in Figure 10.

Figure 11 demonstrates that the input voltage effectively enhances the wear rate, as Rajput V. et al.[39] found. At voltage 17 V, more wear rate occurs than the effect of duty cycle and electrolytic concentration. This happens because the tool surface area gets reduced during voltage conditions. In view of electrolytic concentration, initially, the tool wear rate gets maximum. This is because of the enhanced gas bubble formation, which leads to wear around the cathode tool. The interrelationship between the tool wear rate with its input parameters, such as voltage and electrolytic concentration, is given in Figure 11(a). At minimal voltage conditions, the tool wear rate is increased to 0.270 mg/min and 0.501 mg/min of TWR is obtained at a maximum voltage (19V).

The relation between the duty cycle and the electrolytic concentration rate for analyzing the TWR is shown in

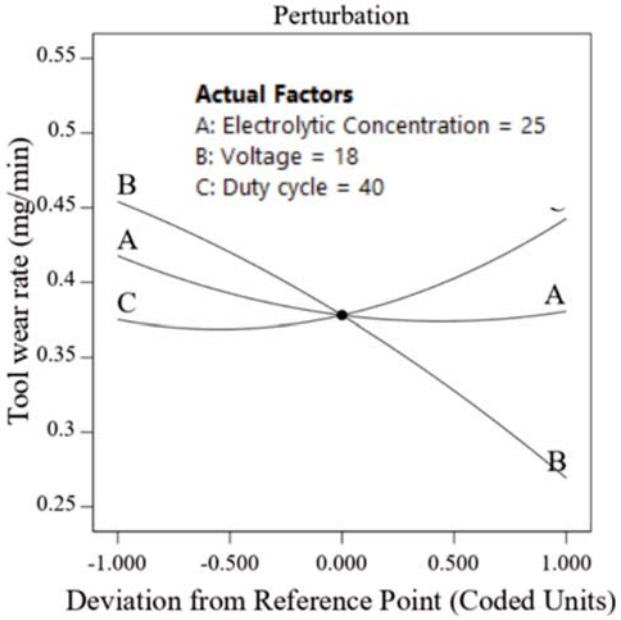

Figure 10. Perturbation of TWR

Figure 11(b). In this, electrolytic concentration helps achieve minimal TWR, and the influence of the duty cycle disturbs the wear rate. This is because the increasing duty cycle tends to enhance the machining time,

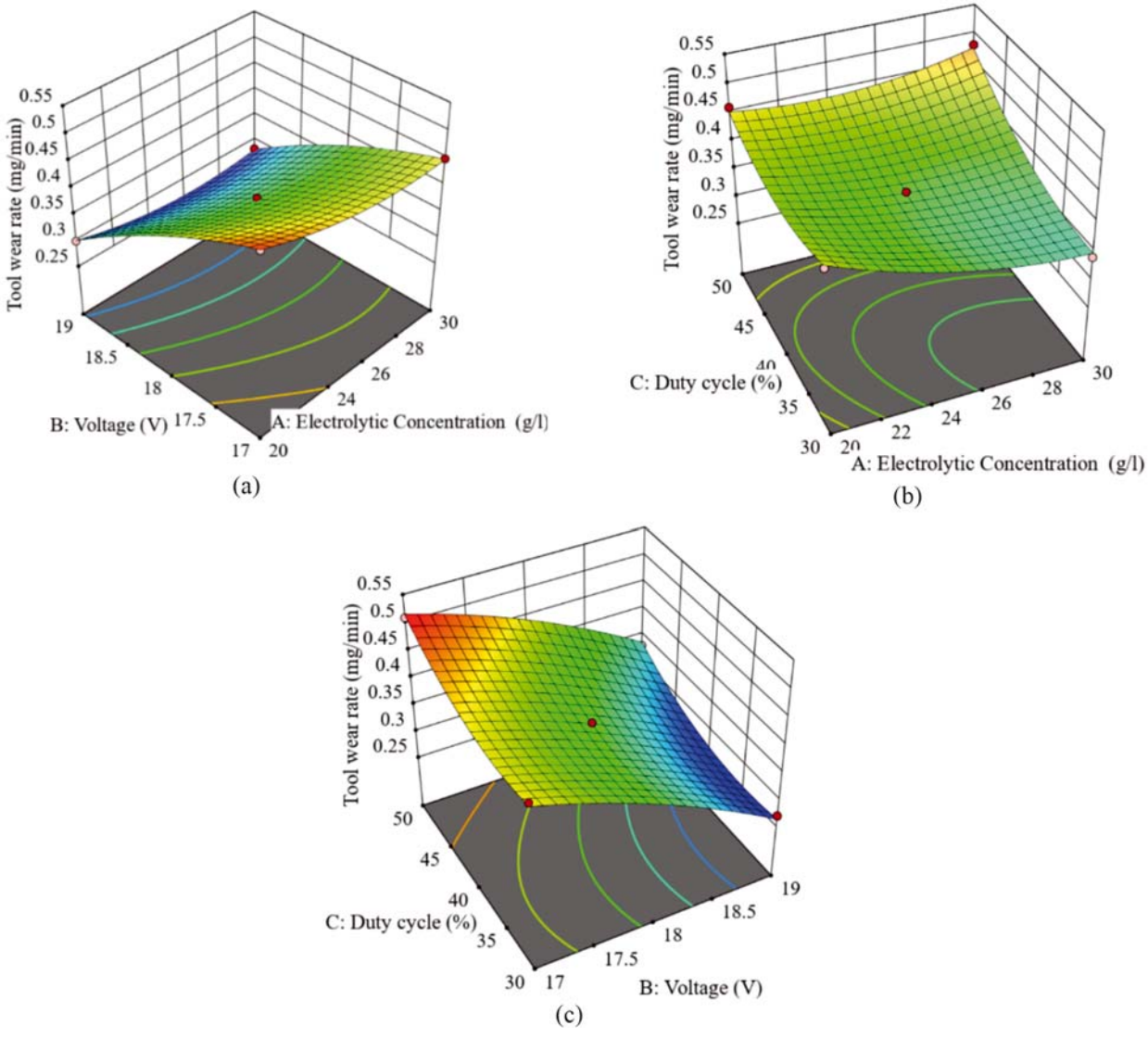

Figure 11. 3D plots of TWR

achieving the maximum tool wear rate of 0.510 mg/min at the duty cycle of 50%. Figure 11(c) represents the 3-D plot for analyzing the influences of voltage and duty cycle on tool wear rate. Compared with the voltage, more wear rate is determined due to the influence of the duty cycle. The analysis reveals that the duty cycle maximizes the tool wear more effectively.

Surface Roughness (SR)

Higher deterioration is created on the surface of the workpiece due to larger cavities by enhanced voltage level. The workpiece can be duplicated only if the electrolytic concentration and the voltage are maintained at the specified value. Uneven surface dissolution and oxide film are produced due to uneven electrical conductivity in the machining gap. Material dissolution is uniform, surface roughness is lower when the voltage is high (19V), but material dissolution is non-uniform, and surface roughness is higher when the voltage is low (17V). The increased duty cycle improves the surface's roughness along the machine's length. Electrolyte products are taken away during the less voltage level by the suitable flow rates. The density and electrolytic concentration are also high during the less voltage level[40]. The Ra of hardened die steel was improved mainly due to the presence of nanoparticles in the electrolyte. Sekar, T. et al.[19] improvised the quality of the finished surface by suspending copper nanoparticles in the electrolyte. Figure 12 represents the perturbation analysis of surface roughness.

The 3D plot representation for analyzing the relationship of machining parameter over the Surface roughness of the die hardened steel is demonstrated in Figure 13. Figure 13(a) represents the effect of voltage and electrolytic concentration over Surface roughness. At the

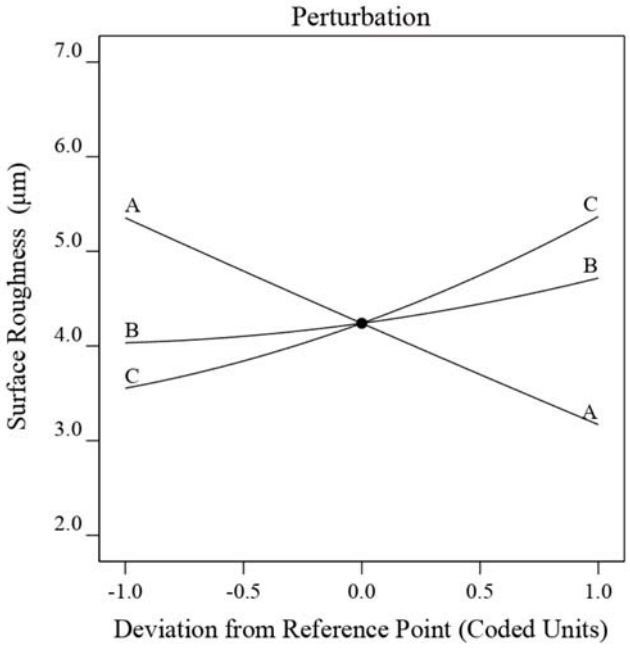

Figure 12. Perturbation plot of surface roughness

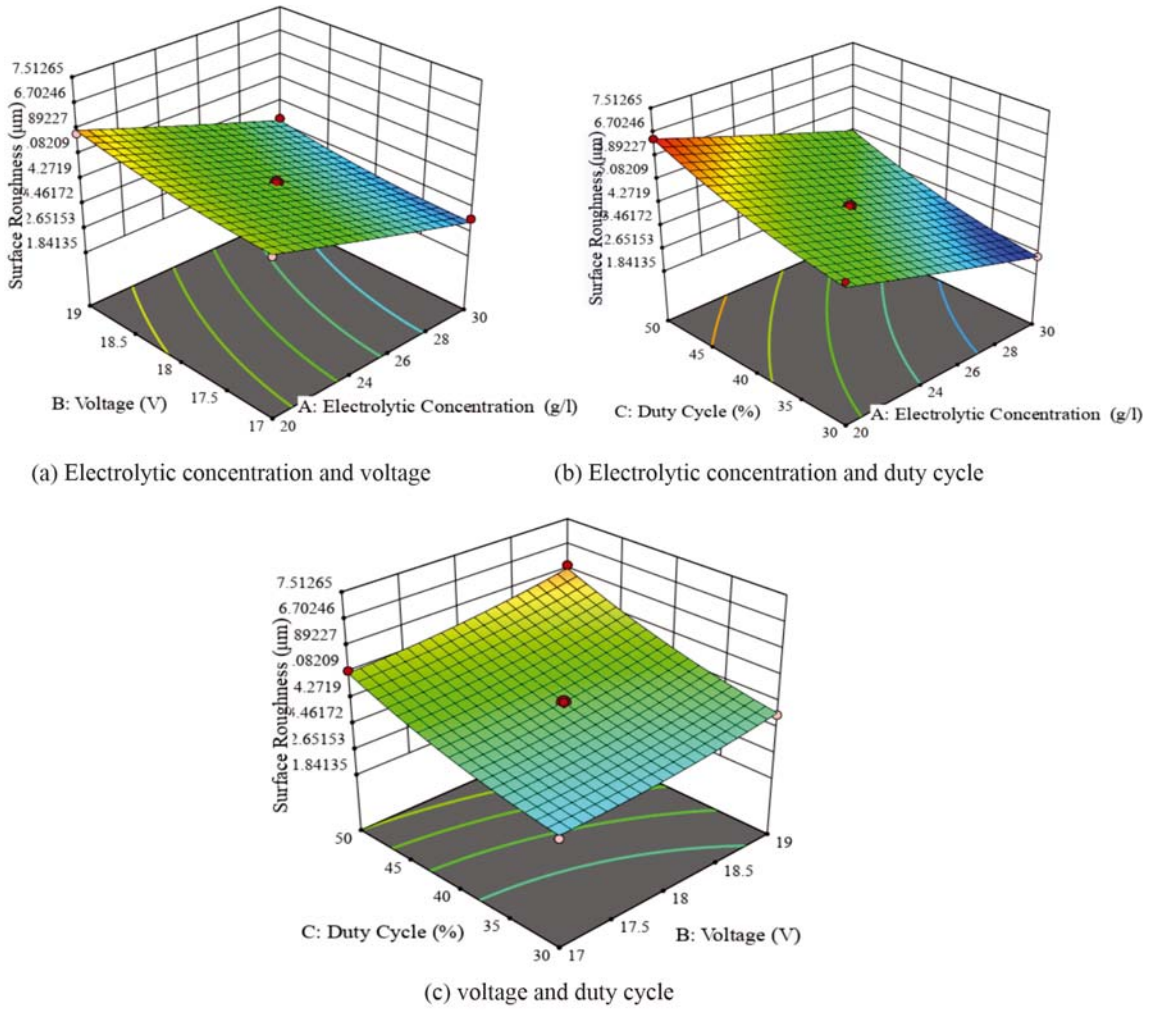

Figure 13. Response surface of surface roughness

30 g/l of electrolyte concentration, 3.68 μm of surface roughness is obtained. The surface roughness behavior is more favorable due to the contribution of voltage. The interrelationship of duty cycle and electrolytic concentration for the surface roughness behavior is given in Figure 13(b). Here, increasing the duty cycle tends to improve the surface roughness. Figure 13(c) reveals the influence of surface roughness over-voltage and duty cycle. Here, more surface roughness is achieved due to the influence of the duty cycle. This is because, by increasing the duty cycle, the machining time and the MRR rate increase, which tends to enhance the Surface roughness. The maximum surface roughness was obtained at 5.8 μm in 50% of the duty cycle and 19 V.

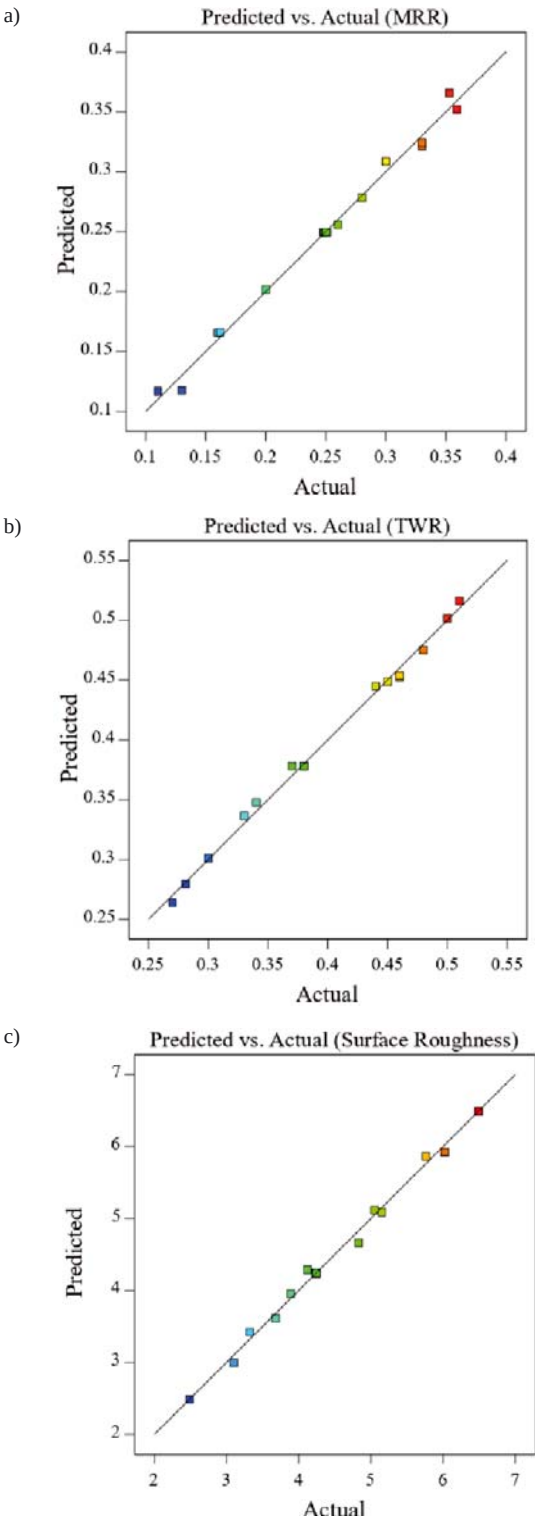

Figure 14. Comparison of actual and predicted results a) MRR, b) TWR, and c) Ra

Prediction of parameters using RSM and Neural network

In this work, the experimented values are predicted using RSM and hybrid DNN based DHO methods. The prediction behaviour is carried out only for the machining activities of optimally selected electrolytic combinations. The predicted result from the response surface methodology for MRR, TWR, and surface roughness are given in Figure 14. In the obtained results from the RSM, the actual and predicted values are founded to be closer to each other. A similar kind of result was noted by Gopinath C. et al.[40] when using the RSM optimization method.

The experimented values are forecasted using our proposed hybrid model for DNN based DHO and are given in Figure 15. In this, the variations between the experimented and the predicted outcomes are much less, and the predicted outcomes are closer to the experimen-

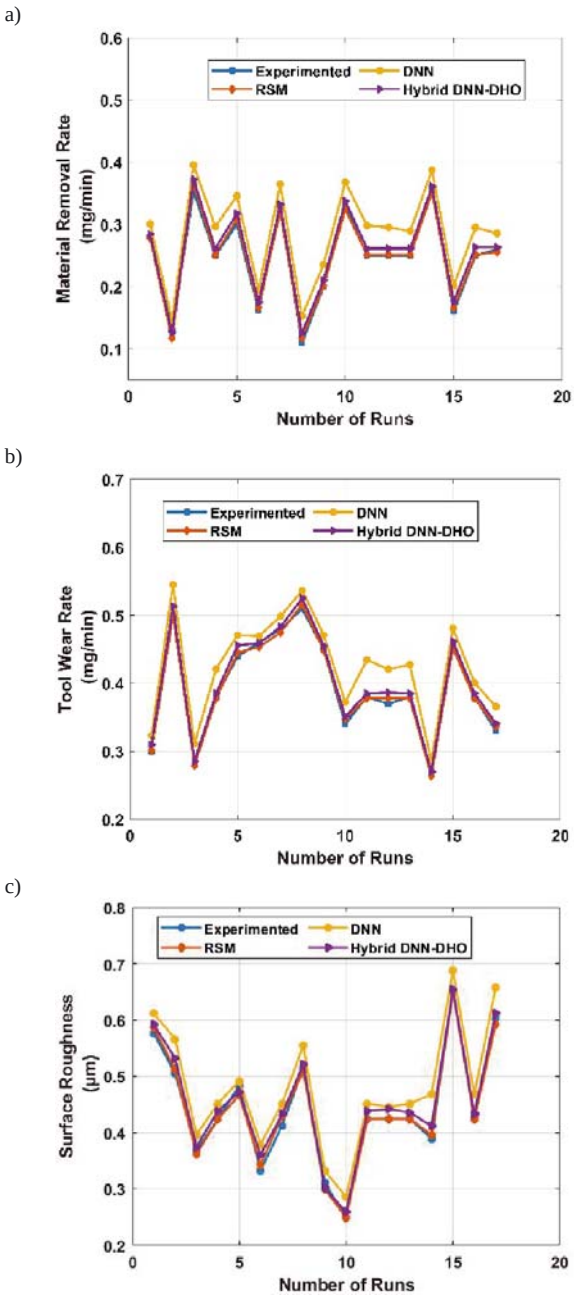

Figure 15. Comparison of predicted values from RSM, DNN-DHO, DNN a) MRR, b) TWR, c) Ra

ted values. Besides, the non-hybrid DNN method is also used to predict the experimented outcomes and compared with our propped method. The optimal predicted value obtained from the hybrid DNN-DHO method for the input condition of 19 V, 20 g/l of EC and 30% DC are 0.361 mg/min of MRR, 0.272 mg/min of TWR, and 2.511 μm of Surface Roughness. The optimal predicted values using RSM are 0.362 mg/min of MRR, 0.269 mg/min of TWR, and 2.662 μm of Ra. When using the non-hybrid DNN, the predicted values for MRR, TWR, and SR are deviate more from the actual outcomes.

Figure 16 represents the regression plot for machining process parameters. The training and validation of these parameters achieve the outcome pertinent to actual values. Compared to experimented results, the DNN--DHO prediction achieves closer results than non-hybrid DNN. The regression coefficient achieved for the MRR is 0.9965, TWR is 0.99742, and surface roughness is 0.99483, respectively. Figure 17 represents the accuracy

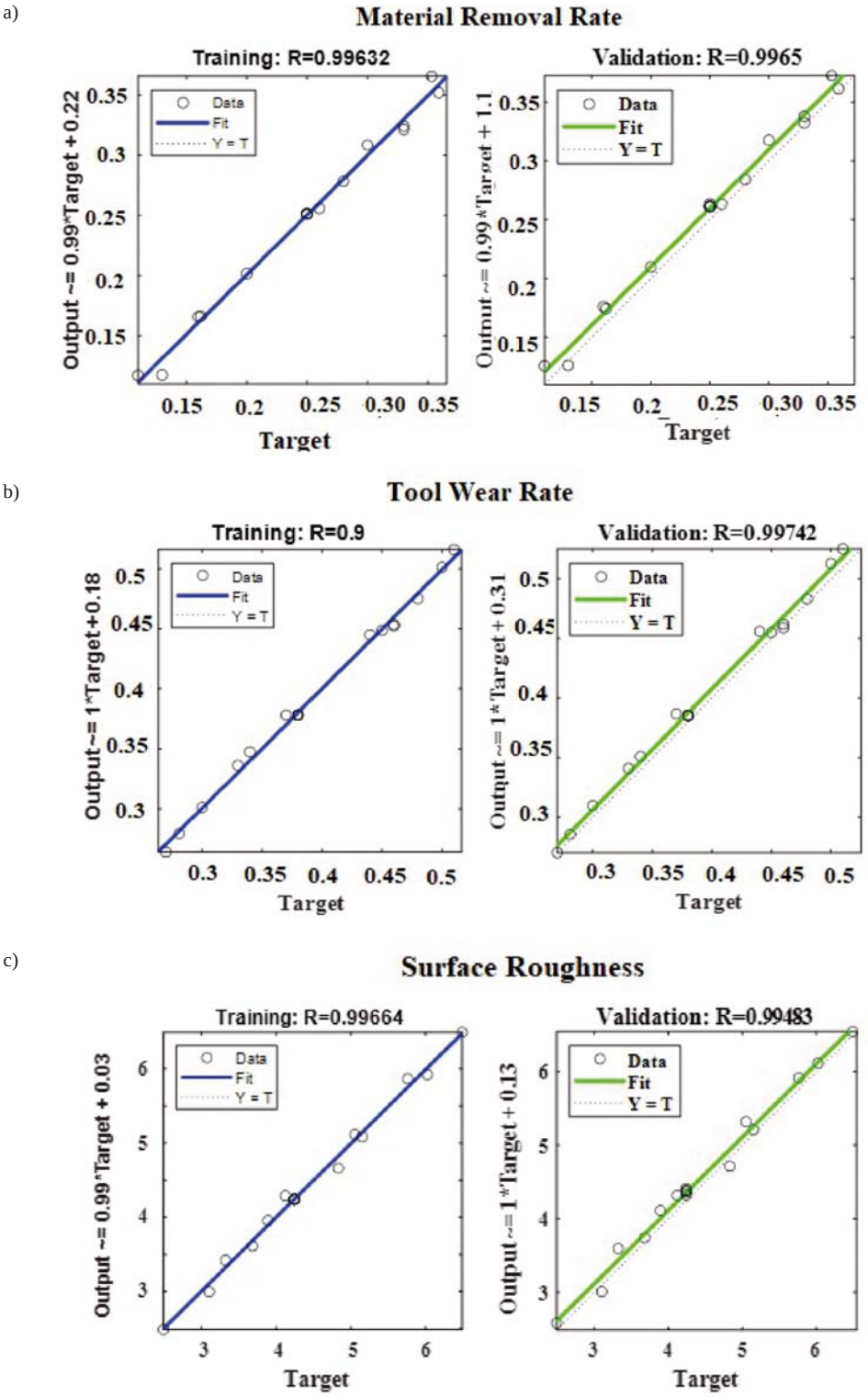

Figure 16. Regression plots for machining performances a) MRR, b) TWR, c) Ra

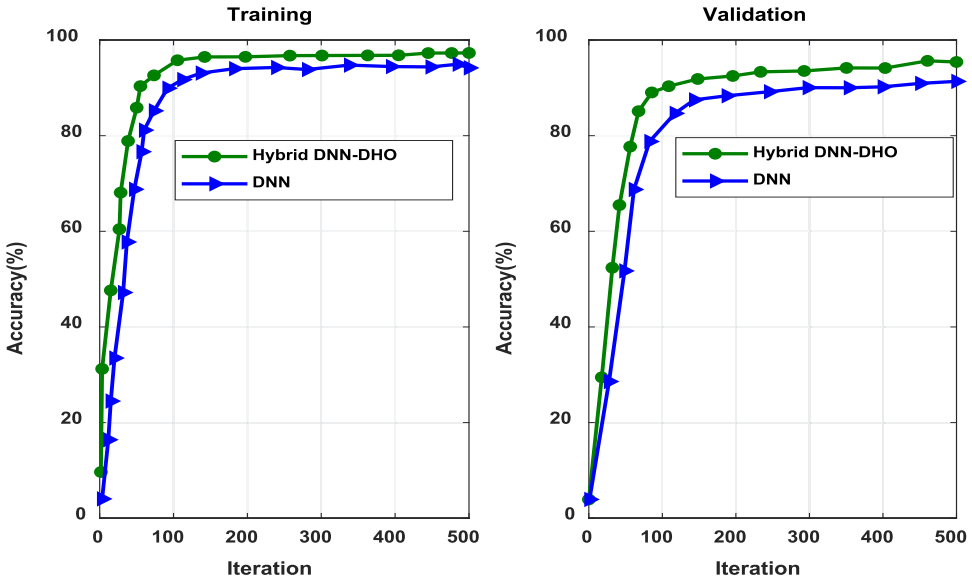

Figure 17. Accuracy of the proposed method and DNN

comparison of training and validation of the DNN and DNN-DHO prediction. The optimal accuracy is obtained in the proposed method of prediction. For DNN prediction, the optimal training accuracy is 89%, and validation is 91%. For hybrid DNN-DHO the optimal accuracy for training is 91%, and validation is 95%.

The error analysis reveals that the proposed prediction model is more favourable than the prediction behaviour of both RSM and DNN. This is because the non-hybrid neural network updates the random weights to forecast the machined outcomes. In the view of the hybrid DNN based DHO prediction model, the weights are initially optimized using DHO and then updated. It proves that the experimented and the predicted values are close and correlated with each other. The Root Mean Square Error (RMSE) analysis for the predicted outcomes of the machined workpiece is shown in Figure 18. The figure shows that the hybrid DNN-DHO promotes a lower error value than the DNN. From the overall machining performances, the error values obtained from Hybrid DNN-DHO are 0.018 to 0.024, and DNN is 0.047 to 0.058. The results of this proposed work are compared with some existing works as given in table 7. The outcomes mainly depend on the properties of the materials and the selected parameters. In ECM machining, tool wear rate analysis is very rarely found. Few works were investigated with the help of nano electrolytes. And several works explained the ECMM characteristics of stainless steel as well.

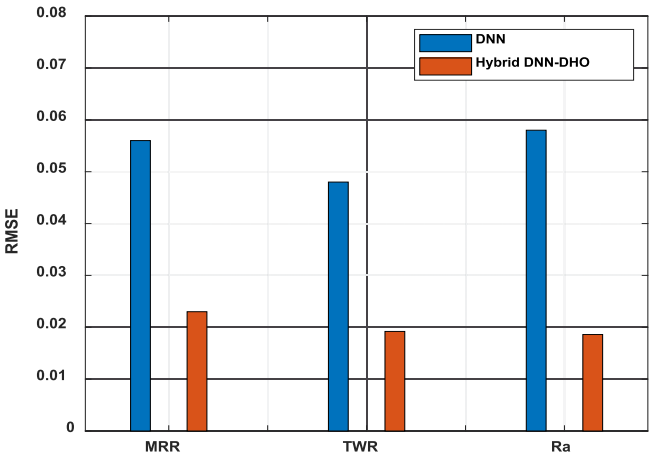

Figure 18. RMSE for hybrid and non-hybrid DNN

CONCLUSION

The ECMM is the most effective method to achieve better surface characteristics and is capable of machining hard materials. In this work, Electrochemical Micromachining has achieved to micro-drill the holes on die hardened steel. The test was conducted by varying six different combinations of electrolytic blends. The experimental model was designed in response to a surface methodology using box Behnken design (RSM-BBD). And then, the results were predicted and validated using the hybrid DNN-DHO technique. The experimental analysis found the optimal electrolyte: stannic oxide and zinc oxide nanoparticles added NaCl. The obtained optimal experimental result was used to train the RSM and hybrid DNN-DHO models. The various observations noticed during ECMM optimization and prediction are as follows,

– The ANOVA table for MRR, TWR, and Ra concludes that the formed quadratic models are well fitted with the experimented outcomes. Specifically, the input

Table 7. Comparison of proposed DNN-DHO with existing methods

Author	Workpiece Material	Electrolyte	MRR (mg/min)	Ra (μm)
Proposed	Hardened die steel	SnO_2 and ZnO added NaCl	0.035	0.035
Krishnan, N., et al. [27]	Stainless steel	$NaNO_3$	0.07	1.343
Panigrahi, D., et al. [28]	Hatelloy	$NaNO_3$	0.063	–
Geethapriyan et al. [12]	Stainless steel	NaCl	0.013	–
Vinod kumar et al. [22]	High chromium die steel	Copper powder added NaCl	0.045	1.39
Gopinath et al. [40]	Duplex stainless steel	$NaNO_3$	0.087	0.44
		$NaClO_3$	0.082	0.49

voltage and electrolyte concentration are more effectively involved in enhancing the machining behaviour.

– The experimental design results in the optimal MRR of 0.359 mg/min and TWR of 0.27 mg/min for 25 g/l of electrolyte concentration, the voltage of 19 V and 30% of duty cycle.

– The ECMM produces a better surface with the surface roughness of 2.49 μm at the electrolytic concentration of 30 g/l, 18 V of voltage and 30% of duty cycle, respectively.

– The RSM predicts the optimum value with the regression coefficients of 0.9927, 0.9955, and 0.9933 for MRR, TWR and Surface roughness.

– The obtained result is comparatively analyzed with hybrid DNN-DHO prediction. The results proved that our proposed algorithm's predicted results were closer to the experimental results. It also achieves a fitness coefficient closer to unity, implying that the designed model is best suited for machining performance prediction and validation.

– The proposed hybrid model starts to produce stable results after 100 iterations while training and validating. Moreover, the proposed hybrid DNN-DHO model achieved 94% overall accuracy with less than 1.5% error.

– The hybridization of the DHO algorithm with DNN significantly improvised the prediction performance of DNN by reducing the RMSE. The obtained RMSE for the proposed DNN-DHO was between 0.018 and 0.024. In contrast, the RMSE of the conventional DNN model ranges between 0.047 and 0.058.

However, the optimization and prediction of ECMM were successfully achieved by the developed hybrid DNN model. The performance of the hybrid DNN model was less than 95%, and this can be improvised in our future studies by implementing some advanced and accurate optimization algorithms. Moreover, only the three output characteristics of MRR, Ra and TWR of ECMM with SnO_2 and ZnO added electrolyte combinations were studied in this work for simplicity. In our future work, more output responses like kerf width, tapper angle, overcut etc., of ECMM with our proposed electrolyte may be investigated using advanced neural network models.

Funding: No funding is provided for the preparation of manuscript.

Conflict of Interest: Authors declare that they have no conflict of interest.

The collected data was incorporated in the manuscript.

LITERATURE CITED

1. Prakash, C., Kansal, H.K., Pabla, B.S. & Puri, S. (2017). Experimental investigations in powder mixed electric discharge machining of Ti–35Nb–7Ta–5Zrβ-titanium alloy. *Materials and Manufacturing Processes*, 32(3), 274–285. DOI: 10.1080/10426914.2016.1198018.

2. Sathish, T. (2019). Experimental investigation of machined hole and optimization of machining parameters using electrochemical machining. *J. Mater. Res. Technol.*, 8(5), 4354–4363. DOI: 10.1016/j.jmrt.2019.07.046.

3. He, H.D., Qu, N.S., Zeng, Y.B. & Yao, Y.Y. (2017). Enhancement of mass transport in wire electrochemical micromachining by using a micro-wire with surface microstructures. *The International J. Adv. Manufact. Technol.,* 89(9), 3177–3186. DOI: 10.1007/s00170-016-9262-4.

4. Sekar, T. & Marappan, R. (2008). Experimental investigations into the influencing parameters of electrochemical machining of AISI 202. *J. Adv. Manufact. Systems*, 7(02), 337–343. DOI: 10.1142/S0219686708001486.

5. Meng, L., Zeng, Y. & Zhu, D. (2017). Investigation on wire electrochemical micro machining of Ni-based metallic glass. *Electrochimica Acta*, 233, 274–283. DOI: 10.1016/j.electacta.2017.03.045.

6. Dong, S., Wang, Z. & Wang, Y. (2017). High-speed electrochemical discharge drilling (HSECDD) for micro-holes on C17200 beryllium copper alloy in deionized water. *The International J. Adv. Manufact. Technol.* 88(1), 827–835. DOI: 10.1007/s00170-016-8645-x.

7. Soundarrajan, M. & Thanigaivelan, R. (2019). Investigation of electrochemical micromachining process using ultrasonic heated electrolyte. *Adv. Micro and Nano Manufact. Surf. Engin., Springer, Singapore*, 423–434. DOI: 10.1007/978-981-32-9425-7_38.

8. Rathod, V., Doloi, B. & Bhattacharyya, B. (2017). Fabrication of microgrooves with varied cross-sections by electrochemical micromachining. *Internat. J. Adv. Manufact. Technol.*, 92(1), 505–518. DOI: 10.1007/s00170-017-0167-7.

9. Anasane, S.S. & Bhattacharyya, B. (2016). Experimental investigation on suitability of electrolytes for electrochemical micromachining of titanium. *Internat. J. Adv. Manufact. Technol.*, 86(5), 2147–2160. DOI: 10.1007/s00170-015-8309-2.

10. Thanigaivelan, R., Arunachalam, R.M., Kumar, M. & Dheeraj, B.P. (2018). Performance of electrochemical micromachining of copper through infrared heated electrolyte. *Mater. Manufact. Proces.*, 33(4), 383–389. DOI: 10.1080/10426914.2017.1279304.

11. Liu, W., Zhang, H., Luo, Z., Zhao, C., Ao, S., Gao, F. & Sun, Y. (2018). Electrochemical micromachining on titanium using the NaCl-containing ethylene glycol electrolyte. *J. Mater. Proces. Technol.,* 255, 784–794. DOI: 10.1016/j.jmatprotec.2018.01.009.

12. Geethapriyan, T., Samson, R.M., Thavamani, J., Arun Raj, A.C. & Pulagam, B.R. (2019). Experimental investigation of electrochemical micro-machining process parameters on stainless steel 316 using sodium chloride electrolyte. *Adv. Manufact. Proces. Springer, Singapore*, 471-480. DOI: 10.1007/978-981-13-1724-8_45.

13. Bhuyan, B.K. & Yadava, V. (2013). Experimental modeling and multi-objective optimization of traveling wire electrochemical spark machining (TW-ECSM) process. *J. Mech. Sci. Technol.,* 27(8), 2467–2476. DOI: 10.1007/s12206-013-0632-7.

14. Sethi, A., Acharya, B.R. & Saha, P. (2022). Electrochemical dissolution of WC-Co micro-tool in micro-WECM using an Eco-friendly citric acid mixed NaNO3 electrolyte. *J. The Electrochem. Soc.,* 169(3), 033503. DOI: 10.1149/1945-7111/ac54d9.

15. Yu, N., Fang, X., Meng, L., Zeng, Y. & Zhu, D. (2018). Electrochemical micromachining of titanium microstructures in an NaCl–ethylene glycol electrolyte. *J. Appl. Electrochem.*, 48(3), 263–273. DOI: 10.1007/s10800-018-1145-y.

16. Tak, M., Reddy S.V., Mishra, A. & Mote, R.G. (2018). Investigation of pulsed electrochemical micro-drilling on titanium alloy in the presence of complexing agent in electrolyte. *J. Micromanufac.*, 1(2), 142–153. DOI: 10.1177/2516598418784682.

17. Ma, N., Phattharasupakun, N., Wutthiprom, J., Tanggarnjanavalukul, C., Wuanprakhon, P., Kidkhunthod, P. & Sawangphruk, M. (2018). High-performance hybrid supercapacitor of mixed-valence manganese oxide/n-doped graphene aerogel nanoflower using an ionic liquid with a redox additive as the electrolyte: *In situ electrochemical x-ray absorption spectroscopy. Electrochimica Acta,* 271, 110–119. DOI: org/10.1016/j.electacta.2018.03.116.

18. Singh, P.K., Das, A.K., Hatui, G. & Nayak, G.C. (2017). Shape controlled green synthesis of CuO nanoparticles through ultrasonic assisted electrochemical discharge process and its

application for supercapacitor. *Mater. Chem. Phys.,* 198, 16–34. DOI: 10.1016/j.matchemphys.2017.04.070.

19. Sekar, T., Arularasu, M. & Sathiyamoorthy, V. (2016). Investigations on the effects of Nano-fluid in ECM of die steel. *Measurement*, 83, 38–43. DOI: 10.1016/j.measurement.2016.01.035.

20. Jiang, K., Wu, X., Lei, J., Wu, Z., Wu, W., Li, W. & Diao, D. (2018). Vibration-assisted wire electrochemical micromachining with a suspension of B4C particles in the electrolyte. *Internat. J. Adv. Manufac. Technol.*, 97(9), 3565–3574. DOI: 10.1007/s00170-018-2190-8.

21. Geethapriyan, T., Muthuramalingam, T., Vasanth, S., Thavamani, J. & Srinivasan, V.H. (2019). Influence of nanoparticles-suspended electrolyte on machinability of stainless steel 430 using electrochemical micro-machining process. *Adv. Manufac. Proces. Sprin., Singap.* 433–440. DOI: 10.1007/978-981-13-1724-8_42.

22. Kumaar, J.R.V., Thanigaivelan, R. & Soundarrajan, M. (2022). A performance study of electrochemical micromachining on SS 316L using suspended copper metal powder along with stirring effect. *Mater. Manufac. Proces.*, 1–14. DOI: 10.1080/10426914.2022.2030874.

23. Yang, Y., Natsu, W. & Zhao, W. (2011). Realization of eco-friendly electrochemical micromachining using mineral water as an electrolyte. *Precision Engin.*, 35(2), 204–213. DOI: 10.1016/j.precisioneng.2010.09.009.

24. Geethapriyan, T., Kalaichelvan, K. & Muthuramalingam, T. (2016). Multi performance optimization of electrochemical micro-machining process surface related parameters on machining Inconel 718 using Taguchi-grey relational analysis. *La Metallurgia Italiana*, 2016(4), 13–19.

25. Fard, A.F. & Hajiaghaei-Keshteli, M. (2016). Red Deer Algorithm (RDA); a new optimization algorithm inspired by Red Deers' mating. *Internat. Confer. Ind. Engin., IEEE* 12, 331–342.

26. Pradeep, N., Sundaram, K.S. & Kumar, M.P. (2020). Performance investigation of variant polymer graphite electrodes used in electrochemical micromachining of ASTM A240 grade 304. *Mater. Manufact. Proces.*, 35(1), 72–85. DOI: 10.1080/10426914.2019.1697445.

27. Krishnan, N., Deepak, J. & Hariharan, P. (2020). Multi-response optimization of electrochemical micromachining on masked SS304. *Engin. Res. Express*, 2(1), 015041. DOI: 10.1088/2631-8695/ab5eb9.

28. Panigrahi, D., Rout, S., Patel, S.K. and Dhupal, D. (2021). Stray current and its consequences on microstructure of Hastelloy C-276 during parametric investigation on geometrical features: fabricated by electrochemical micromachining. *Internat. J. Adv. Manufact. Technol.*, 112(1), 133–156. DOI:10.1007/s00170-020-06365-9.

29. Prakash, J. & Gopalakannan, S. (2021). Teaching—learning-based optimization coupled with response surface methodology for micro electrochemical machining of aluminium nanocomposite. *Silicon*, 13(2), 409–432. DOI: 10.1007/s12633-020-00434-0.

30. Ranganayakulu, J., Srihari, P.V. & Rao, K.V. (2021). An optimization strategy to improve performance in electrochemical discharge machining of borosilicate glass using graph theory algorithm and desirability index. *Silicon*, 1–14. DOI: 10.1007/s12633-021-01317-8.

31. Gautam, N., Goyal, A., Sharma, S.S., Oza, A.D. & Kumar, R., 2022. Study of various optimization techniques for electric discharge machining and electrochemical machining processes. *Materials Today: Proceedings*, 57, 615–621. DOI: 10.1016/j.matpr.2022.02.005.

32. Aslan, N.E.V.Z.A.T. & Cebeci, Y.A.K.U.P. (2007). Application of Box–Behnken design and response surface methodology for modeling of some Turkish coals. *Fuel*, 86(1–2), 90–97. DOI: 10.1016/j.fuel.2006.06.010.

33. Barabadi, H., Honary, S., Ebrahimi, P., Alizadeh, A., Naghibi, F. & Saravanan, M. (2019). Optimization of mycosynthesized silver nanoparticles by response surface methodology employing Box-Behnken design. *Inorganic and Nano-Metal Chemistry*, 49(2), 33–43. DOI: 10.1080/24701556.2019.1583251.

34. Kim, S.G., Harwani, M., Grama, A. & Chaterji, S. (2016). EP-DNN: a deep neural network-based global enhancer prediction algorithm. *Scientific reports*, 6(1), 1–13. DOI: 10.1038/srep38433.

35. Brammya, G., Praveena, S., Ninu Preetha, N.S., Ramya, R., Rajakumar, B.R. & Binu, D. (2019). Deer hunting optimization algorithm: a new nature-inspired meta-heuristic paradigm. *Comp. J*. DOI: 10.1093/comjnl/bxy133.

36. Elhami, S. & Razfar, M.R. (2020). Application of nano electrolyte in the electrochemical discharge machining process. *Precision Engin.*, 64, 34–44. DOI: 10.1016/j.precisioneng.2020.03.010.

37. Teimouri, R. & Sohrabpoor, H. (2013). Application of adaptive neuro-fuzzy inference system and cuckoo optimization algorithm for analyzing electro chemical machining process. *Front. Mech. Engin.*, 8(4), 429–442. DOI: 10.1007/s11465-013-0277-3.

38. Charak, A. & Jawalkar, C.S. (2020). Experimental studies in micro channelling on borosilicate glass using RSM optimization technique. *Silicon*, 12(7), 1707–1721. DOI: 10.1007/s12633-019-00269-4.

39. Rajput, V., Goud, M. & Suri, N.M. (2021). Performance analysis of closed-loop electrochemical discharge machining (CLECDM) during micro-drilling and response surface methodology based multi-response parametric optimization. *Adv. Mater. Process. Technol.*1–31. DOI: 10.1080/2374068X.2020.1860494.

40. Gopinath, C., Lakshmanan, P. & Amith, S.C. (2021). Production of Micro-holes on Duplex Stainless Steel 2205 by Electrochemical Micromachining: A Grey-RSM Approach. *Arabian J. Sci. Engin.*, 46(3), 2769–2782. DOI: 10.1007/s13369-020-05277-w.